The Seismic Record
A journal of the Seismological Society of America

Leakage During Hydropower Tunnel Construction: A Possible Trigger Mechanism for the Earthquake Swarm at Sørfjorden, Norway

OPEN ACCESS

Angélique Marck*[1,2], Lars Ottemöller[1], Gökhan Aslan[3], Odleiv Olesen[3], and Stéphane Rondenay[1]

Abstract

Earthquake swarms are often linked to variations in subsurface fluid pressures, driven by natural processes or anthropogenic activity. Here, we investigate whether an earthquake swarm in Nordland, a region in northern Norway, was possibly related to the construction of a hydropower tunnel. Using Interferometric Synthetic Aperture Radar, we observe subsidence following the tunnel's construction, which can be explained by significant water leakage encountered during the work. Three years later, an earthquake swarm occurred about 3 km from the tunnel, in an area without previous swarm activity. We build a catalog of the swarm and through analysis of its spatio-temporal distribution propose that changes in pore pressure and stress, potentially linked to the leakage, may have played a role in triggering the swarm. Fault valving or pumping are possible mechanisms to explain the cascading nature of the earthquakes in the swarm.

Cite this article as Marck, A., L. Ottemöller, G. Aslan, O. Olesen, and S. Rondenay (2026). Leakage During Hydropower Tunnel Construction: A Possible Trigger Mechanism for the Earthquake Swarm at Sørfjorden, Norway, *The Seismic Record*. **6**(**1**), 44–53, doi: 10.1785/0320250045.

Introduction

Both natural and anthropogenic changes in fluid pressure can play a significant role in triggering earthquakes. In the hydrocarbon industry, both extraction of hydrocarbons and injection of fluids can induce or trigger seismicity (McGarr *et al.*, 2002; Ellsworth, 2013). Other industries that inject fluids with the potential to trigger earthquakes include geothermal energy production and wastewater disposal (Ellsworth, 2013). Demonstrating that seismicity is caused by anthropogenic changes can be challenging. Poroelastic modeling of stress and pore pressure can be utilized to understand the relation between fluid injection and seismicity (Segall and Lu, 2015).

Fault valving, where a barrier is broken due to a pressure gradient and fluid movement happens during the earthquake (Sibson, 1981), was suggested as a possible mechanism driving an earthquake swarm at the Long Valley caldera (Shelly *et al.*, 2016), and also as a possible initiation of the Cahuilla, California, swarm (Ross *et al.*, 2020). Ross *et al.* (2020) demonstrated that the Cahuilla swarm occurred in response to infiltration of fluids into the fault system from a deeper reservoir. Their suggested injection point was at the bottom of the swarm, from where fluids migrated through permeable fault zones. Furthermore, fluid transients combined with a valving mechanism were presented as a model for low-frequency earthquakes on the Guerrero subduction zone interface (Farge *et al.*, 2021). In their model, a pressure gradient results in a change of permeability, allowing for rapid fluid flow that is then followed by clogging of the fault zone. This mechanism can explain observed seismograms and represents a viable alternative to the more conventional invoked process of shear slip (Shapiro *et al.*, 2018).

Anthropogenic changes in external load present another mechanism to trigger or induce earthquakes. There are many examples where load changes during the initial filling of

1. Department of Earth Science, University of Bergen, Bergen, Norway, https://orcid.org/0009-0003-5219-9162 (AM); https://orcid.org/0000-0003-3170-1048 (LO); https://orcid.org/0000-0003-0805-249X (SR); 2. Now at Helmholtz Centre Potsdam, GFZ German Research Centre for Geosciences, Potsdam, Germany; 3. Geological Survey of Norway (NGU), Trondheim, Norway, https://orcid.org/0000-0001-9482-4382 (GA)

*Corresponding author: amarck@gfz.de

reservoirs or due to variation in water level cause seismicity (Talwani, 1997). Groundwater extraction that resulted in surface subsidence has been linked to earthquakes in Spain, where the cause was thought to be unloading (González *et al.*, 2012). A swarm of earthquakes in Israel was attributed to dilational stress changes at a permeability boundary resulting from groundwater pumping (Wetzler *et al.*, 2019). Water inflow during tunnel construction and related fluid migration were identified as the likely cause of induced seismicity near the Hongtu tunnel in China (Ma *et al.*, 2025).

Here we describe the possibility that an earthquake swarm at Sørfjorden, in the Nordland region of Norway, was anthropogenically triggered by fluid pressure changes caused by the construction of a hydropower tunnel system. Our investigation shows that the leakage was significant enough to cause surface subsidence that was observed with Interferometric Synthetic Aperture Radar (InSAR) data. We resolve the spatiotemporal evolution of the earthquake swarm that initiated after tunnel completion. We present a hypothetical model for the swarm that would initiate because of an increase in fluid pressure differential at the edge of the swarm volume. Such a model may raise the possibility that other swarms in the region can be explained in a similar way.

Background

The Nordland region is one of the most seismically active areas in Fennoscandia (Hicks *et al.*, 2000; Shiddiqi *et al.*, 2022), where the largest known earthquake of magnitude 5.8 on mainland Norway occurred in 1819. Much of the seismicity onshore along the Nordland coast occurs as earthquake swarms. Fault-plane solutions and spatial distribution of events have been associated with north-northeast–south-southwest (NNE-SSW)-trending normal faults (Hicks *et al.*, 2000; Shiddiqi *et al.*, 2023). The shallow earthquakes are likely due to glacial isostatic adjustment and erosion processes, rather than the regional mid-Atlantic ridge push force (Hicks *et al.*, 2000; Gradmann *et al.*, 2024). Recently, the spatiotemporal evolution of the ongoing Jektvik swarm was resolved in detail, allowing for the identification of several clusters (Shiddiqi *et al.*, 2023). The swarm was attributed to shallow fluid saturated fracture zones (Shiddiqi *et al.*, 2022, 2023) and possibly modulated in time by hydrological load changes (Shiddiqi *et al.*, 2023).

The Nordland region is the focus of this study, with the investigated earthquake swarm located near the settlement of Sørfjorden on the eastern side of the fjord with the same

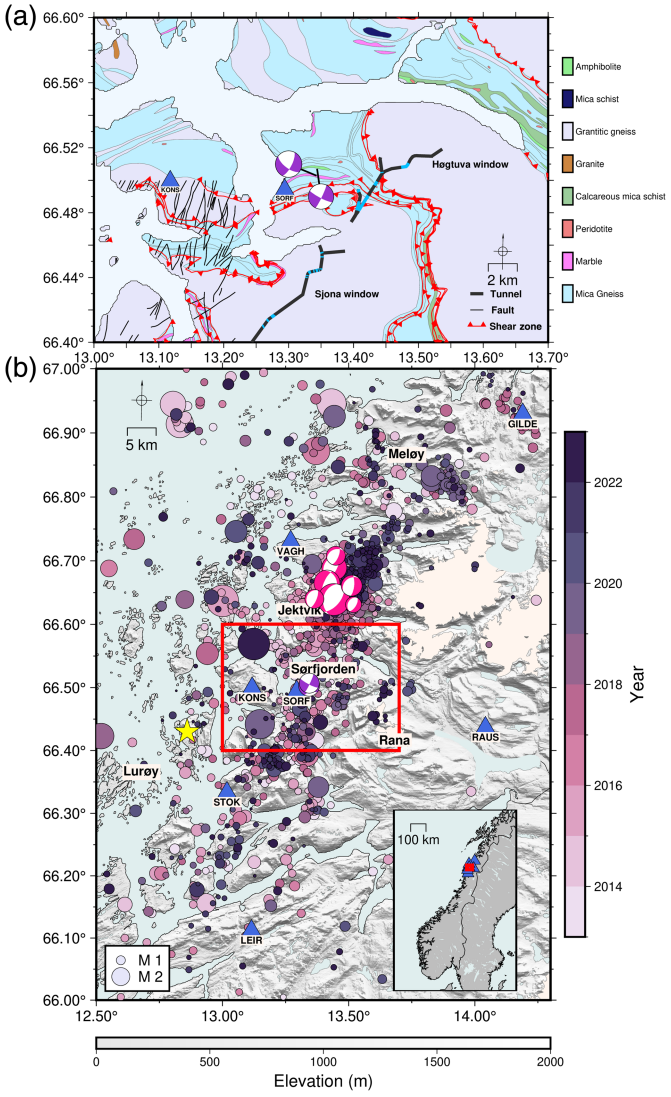

Figure 1. (a) Geological map of the study area, modified from the Geological Survey of Norway, showing mapped shear zones and faults. Note that fault mapping in the region is incomplete. Earthquake focal mechanisms denoted by purple circles were calculated in this study. The blue triangles indicate the location of the seismic stations. The thick gray line represents the tunnel trace, with the blue section indicating the area where high leakage was reported. (b) The shaded relief map of Nordland from Kartverket, showing the NNSN seismic catalog from 2013 to 2023, the Svartisen glacier, and all seismic stations used in this study (blue triangles). The yellow star marks the estimated epicenter of the Lurøy earthquake. The Sørfjorden study area is indicated by the red box. The pink focal mechanisms north of Sørfjorden are from Shiddiqi *et al.* (2022).

name. Geologically, the region belongs to the northern part of the central domain of the Scandinavian Caledonides, which resulted from continental collision during the Silurian to Devonian periods and developed a stack of nappe complexes

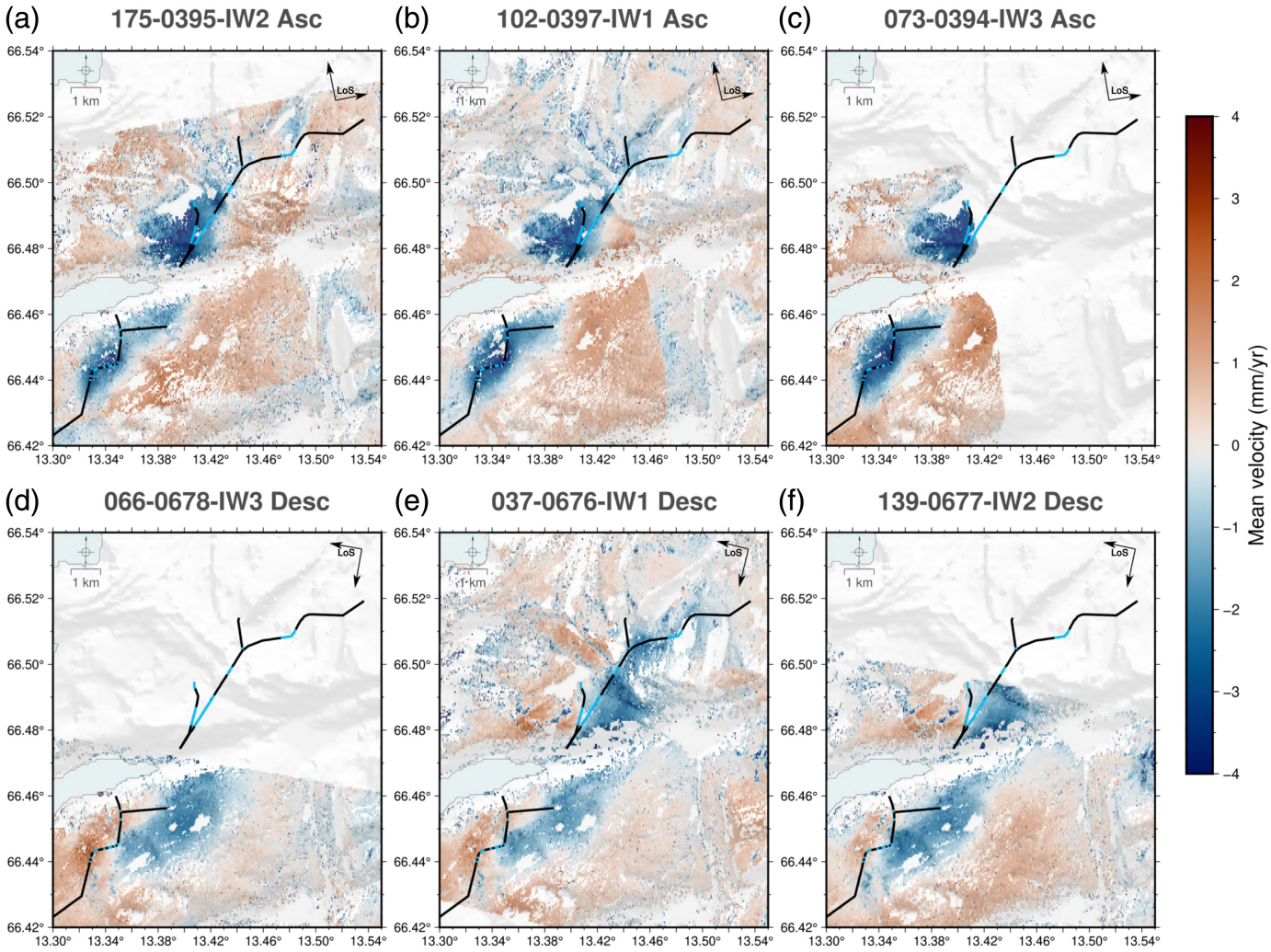

Figure 2. Sentinel-1 PS-Interferometric Synthetic Aperture Radar (InSAR) mean line-of-sight (LoS) velocity fields derived over the period 2015–2019 for ascending tracks (a–c) and descending tracks (d–f). The arrows indicate LoS and flight directions of the satellite. Positive values indicate motion toward the satellite, while negative values indicate motion away from it. The thick black line represents the tunnel trace, with the blue section indicating the area where high leakage was reported.

(Corfu *et al.*, 2015). In the Sørfjorden area, the bedrock geology (Fig. 1) in the southern part is dominated by pre-Cambrian granitic and mica gneiss, which are separated by shear zones. In the northern part, Caledonian-age mica slates are overthrusted onto basement rocks and separated along shear zones from units of gneiss to the east. Discontinuities are clearly visible in the area, in particular along the shear zones, from aerial photographs (Haugerud, 2020) and digital elevation data.

Hydropower is the main source of electricity in Norway, contributing about 90% of the total production. This is achieved through more than 1700 hydropower plants, relying on over 4000 km of waterway tunnels. Most of the hydropower plants were established before 1990, but new infrastructure has been developed in recent years. One such project is the SmiSto hydropower development, which involved the excavation of tunnels to Storåvatn, a few kilometers east of Sørfjorden. As with other similar projects, geological investigations were required at Storåvatn before and during tunnel construction, to avoid complications associated with rock quality or weakness zones.

The SmiSto hydropower project consists of two separate catchments. Our focus is on the Storåvatn part with a capacity of 35 MW, located north of the Gjervalen fjord (Fig. 1) (Haugerud, 2020). The construction began in June 2015 and was completed in September 2020. A main tunnel of 8.6 km length and a shorter branch tunnel of 2 km connect to several

water reservoirs (Haugerud, 2020). The Storåvatn tunnels cross several shear zones, which became problematic during construction (Haugerud, 2020). Various sets of water-conducting joints and highly weathered fracture zones were observed along the tunnel (Haugerud, 2020). Considerable water leakage with inflow rates exceeding 16 l/s, which are high compared with inflow rates in other tunnels (e.g., 8 l/s in the Gotthard tunnel, Loew *et al.*, 2015), caused construction delays (1.5 yr) and necessitated additional grouting to seal inflows after excavation (Haugerud, 2020). High leakage (Fig. 1) was confined to specific times between spring 2016 and summer 2020 and ceased with the additional grouting. The total grouting cement consumption was 19 times higher than expected (Haugerud, 2020).

Surface deformation observed from InSAR data

Sentinel-1 persistent scatterer (PS)-InSAR data from the Norwegian Ground-Motion Service reveal subsidence above the tunnels constructed in the SmiSto hydropower project. We analyzed these data to quantify the magnitude, spatial extent, and timing of the deformation. Our primary analysis used ascending track 102 and descending track 37, which together cover the area of interest and allow decomposition of the line-of-sight (LoS) velocities into east–west and vertical components. In addition, four supplementary tracks (ascending 175 and 73; descending 66 and 139) partly overlap the study area and are used to confirm the consistency of the observed deformation patterns. We analyzed the deformation from 2015 to 2024.

The Sentinel-1 datasets were processed using a persistent scatterer interferometry (PS-InSAR) workflow implemented in the GSAR-GTSI system developed by NORCE, within the framework of the Norwegian Ground Motion Service (Dehls *et al.*, 2019). The processing follows the principles of PS-InSAR (Ferretti *et al.*, 2001) and is optimized for Sentinel-1's TOPS acquisition mode. All scenes were coregistered using an enhanced spectral diversity (ESD) approach (Prats-Iraola *et al.*, 2012), ensuring subpixel alignment across bursts. Acquisitions from winter months were excluded from the analysis to reduce decorrelation effects related to snow accumulation and melt. Interferograms were generated using a single-reference network, and topographic phase contributions were removed using the 3-arcsecond Shuttle Radar Topography Mission digital elevation model. Mean LoS velocities and displacement time series were then estimated for each persistent scatterer, with all results referenced to a stable area outside the deformation zone. The resulting mean LoS velocity maps, over the period 2015–2019, for all processed tracks are shown in Figure 2.

Localized deformation is clearly detected around the tunnel area. The consistent spatial pattern observed across independent ascending and descending acquisitions confirms that the signal represents actual ground deformation rather than noise. The other datasets did not reveal any consistent deformation patterns, indicating that ground motion ceased after 2019. The main subsidence zone aligns closely with the tunnel track and extends over several hundred meters on both sides. Because the ascending and descending datasets have different acquisition geometries, they were used jointly to decompose LoS velocities into vertical and east–west components, based on tracks 102 and 37, following the approach described by Wright *et al.* (2004).

Spatiotemporal evolution of the earthquake swarm

The earthquake swarm at Sørfjorden started on 19 June 2023 (Figs. 3 and 4) and lasted until mid-2024, whereas most of the seismic energy was already released during July 2023 (Fig. 3). A significant part of the activity occurred in bursts, with peaks in event rate of almost 300 events per day (Fig. 3). The largest event had a local magnitude $M_L = 2.1$, whereas the equivalent moment magnitude for the whole swarm is approximately M_w 2.5 (Fig. 3).

Detailed spatiotemporal mapping of seismicity is essential when considering underlying physical models. To improve event detection and relative location accuracy, we utilized the software packages EQcorrscan (Chamberlain *et al.*, 2017) and hypoDD (Waldhauser, 2001), respectively. We used data from six permanent stations located in the region and one local temporary station, SORF, that was installed a few kilometers from the swarm on 14 August 2023. These stations belong to the NS seismic network operated by the University of Bergen. They were equipped with 120 s broadband sensors and recorded with a sampling rate of 100 Hz (Fig. 1).

As common for earthquake swarms, nearly colocated events had similar waveforms, which allowed us to employ matched-filter detection methods implemented in RobustRAQN and EQcorrscan (Chamberlain *et al.*, 2017). Waveforms for well-defined events were selected as templates, which were then used to detect new events in continuous data by computing cross-correlation between the template and the data (Chamberlain *et al.*, 2017). We utilized 481 events of magnitude M_L ranging from −1.3 to 2.1 from the Norwegian National seismic network (NNSN) catalog of this swarm to create templates. The template events were detected on at least three stations and had a signal-to-noise ratio ≥2. The data were filtered between 3 and 12 Hz.

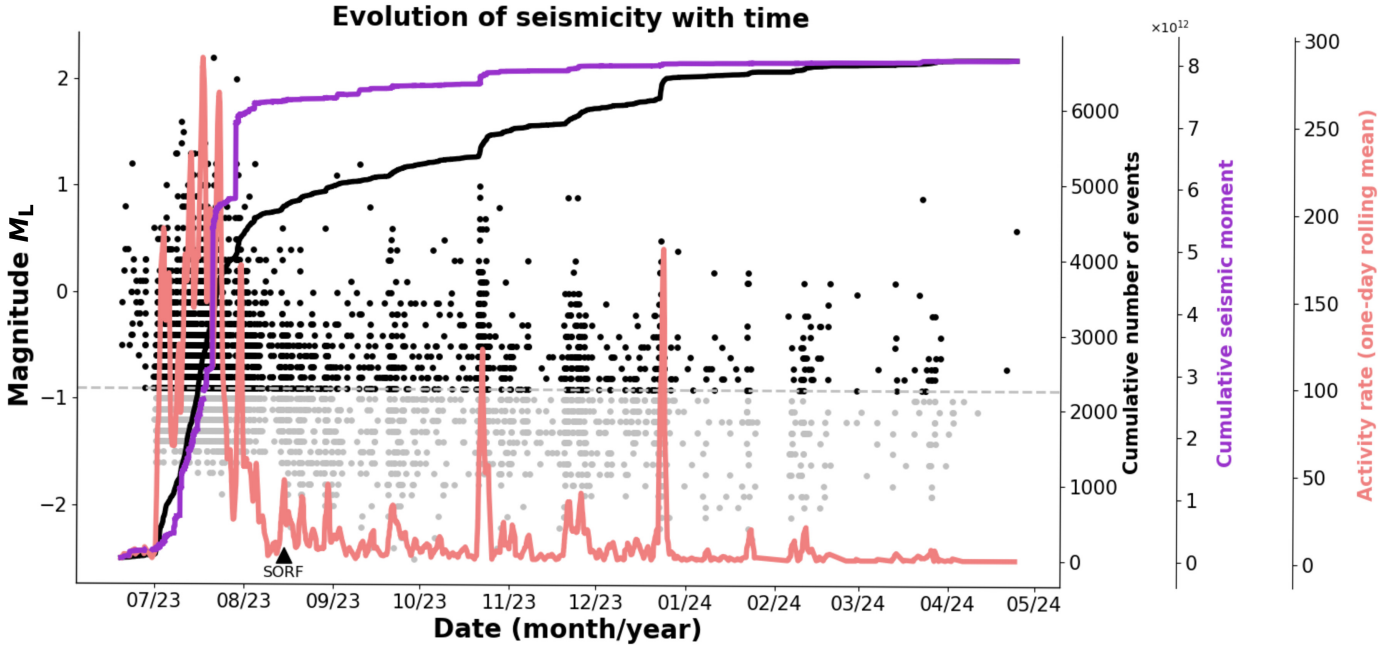

Figure 3. Evolution of seismicity over time. The black dots represent the magnitudes of events, the black curve shows the cumulative number of events, the purple curve indicates the cumulative seismic moment (N · m), and the coral curve represents the activity rate, calculated using a one-day rolling window. Events under the magnitude of completeness are represented in gray. The black triangle indicates the date when the seismic station SORF was installed.

For detection, we set a mean absolute deviation (MAD) threshold of 16, and required detections to be identified on at least six channels across three stations. Arrival-time picks were made if the cross-correlation was ≥0.9. This process yielded 6658 detected events. Local magnitudes for these events were automatically measured.

Preliminary locations computed with the HYPOCENTER program (Lienert *et al.*, 1986) were found to be poorly constrained in east–west (E–W) direction due to station distribution. To address this issue, we set initial locations of all events to the center of the cluster (taken from the NNSN catalog) and initial depths to 3 km. Events above the magnitude of completeness $M_c \geq -0.9$ of our automatic catalog, calculated using the maximum curvature approach (Woessner and Wiemer, 2005), were then relocated using hypoDD (Waldhauser, 2001) (Fig. 4). We conducted synthetic tests to ensure that hypoDD could accurately resolve the swarm structure with all events initially collapsed into the center of the swarm. Synthetic events were generated along a north–south (N-S) plane, approximating the cluster recorded in the NNSN catalog, and subsequently relocated to the cluster's center. After running hypoDD, the original locations along the plane were recovered, also after introducing noise comparable with the expected picking errors.

We were able to relocate 1833 from 3594 events above M_c. Uncertainties were assessed by recalculating locations and determining their error ellipsoids from 100 resampled differential travel-time datasets, each with 10% of the data removed. The mean uncertainties in longitude, latitude, and depth are 0.33, 0.16, and 0.54 km, respectively.

To interpret the spatio-temporal evolution of the swarm, we need to clarify which patterns are robust. First, we assessed whether the number of events detected (6658) was representative of the swarm. To do this, we evaluated the template matching detections by checking the false detection rate on a subset of the detected events. About 6% of the randomly reviewed events were not visibly identifiable in the waveforms, but considered to be real events and kept in the following analysis (Halpaap *et al.*, 2024). Given this, we are confident in the validity of the detections. Our hypoDD locations were based on both manual and automatic picks. We compared manual and automatic picks for 200 events and observed standard deviations of 0.21 and 0.23 s for the *P*- and *S*-wavepick differences, respectively. These timing differences translated into standard deviations of 0.8 km in longitude, 0.3 km in latitude, and 1.2 km in depth between the manual and automatic relocated catalogs. Considering the relative location

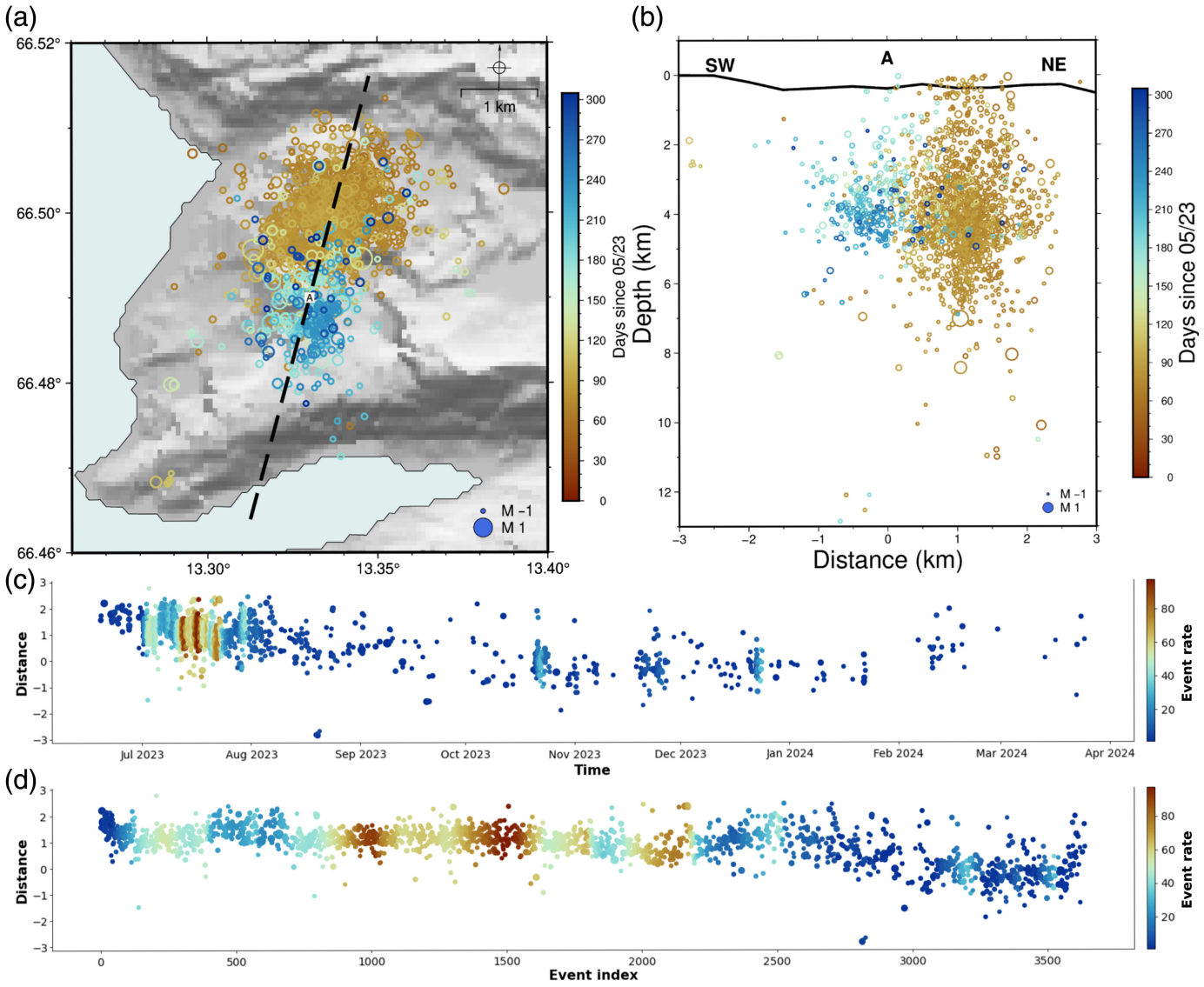

Figure 4. (a,b) Map and cross-section illustrating the relocated catalog of the swarm. Events are color-coded by date (days since 01/05/2023) and scaled by magnitude. (c,d) Distance along section A, thanks to time (c) and event index (d), color-coded by event rate calculated using a one-day rolling window. The distance scale is going from southwest (SW) −3 km to northeast (NE) 3 km.

uncertainties, we are confident in the overall distribution pattern rather than precise individual positions.

From the spatial distribution of events in Figure 4, we identify a NNE-SSW alignment of the swarm, with clear migration from NNE to SSW between July–August 2023 and October–November 2023. Although we cannot rule out the possibility that events are aligned along a sharply defined fault plane, it seems more likely that they are distributed within a broader ellipsoidal volume. We observe minor back-and-forth migration along the NNE-SSW axis during July and August (Fig. 4). The first events (from 0 to about 100) migrate toward the SE, followed by a small shift back to the northwest (NW) between roughly events 400 and 500. After event 700, the earthquakes generally migrate toward the southeast (SE). At approximately event 2200, the swarm appears to shift back to the NW before clearly resuming migration toward the SE.

For the two events with magnitudes exceeding 2, we calculated fault-plane solutions using first-motion *P*-wave polarities (7 for each event) via the HASH software (Hardebeck and Shearer, 2002). Their focal mechanisms with uncertainties have strike, dip, and rake as 127° ± 7°/65° ± 29°/157° ± 29°

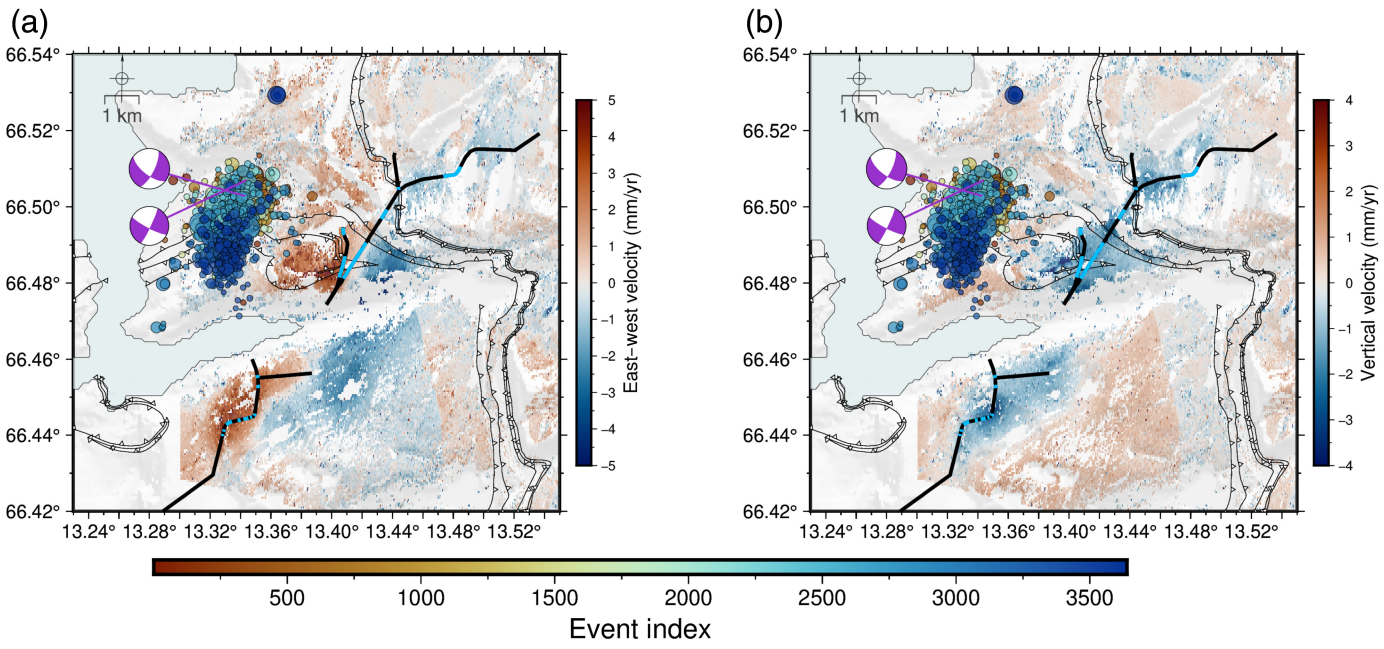

Figure 5. InSAR velocity maps showing east–west (a) and vertical (b) components, alongside the relocated earthquake catalog for Sørfjorden. Earthquakes are color-coded by event index. The thick black line represents the tunnel trace, with the blue section indicating the area where high leakage was reported. Shear zones are delineated by thinner black lines with white triangles.

and 117° ± 20°/80° ± 30°/173° ± 28°. These focal mechanisms carry significant uncertainties as they are based on only seven polarities and a limited station distribution. However, they suggest either strike-slip or normal motion, with one nodal plane aligned along a NNE-SSW structure that follows the swarm orientation and which is consistent with previous swarms in the area (Shiddiqi *et al.*, 2022).

Discussion

In the preceding sections, we presented geodetic and seismological observations from the Sørfjorden area, where hydropower tunnels were constructed between 2015 and 2020, and a swarm of several thousand small events began in June 2023. Although the results carry uncertainties, as presented earlier, the main observations remain robust within those bounds and can be summarized as follows. First, significant water leakage was encountered from spring 2016 in the subsurface during the Storåvatn tunnel construction, indicating the presence of fluids and good conductivity through faults and joints. Second, InSAR measurements show substantial surface deformation between 2015 and 2019. The decomposed vertical and E–W displacement components (Fig. 5) show patterns consistent with tunneling-induced ground movement. The vertical component reveals localized subsidence of up to 5 mm/yr aligned with the tunnel. The E-W component displays a symmetric convergence pattern toward the tunnel trace. The deformation signal extends several hundred meters on both sides of the tunnel trace, consistent with a spatially diffuse response of the fractured rock mass to localized pressure reduction. Third, an earthquake swarm started about 3 yr after tunnel construction, with a 3-km-long alignment in NE-SW direction at depths of 1–7 km. In this section, we propose a model to connect these observations.

Earthquake swarms are quite common in the Nordland region of Norway, and the Sørfjorden swarm may not seem very different from the earlier swarm at Steigen and the ongoing swarm at Jektvik (Shiddiqi *et al.*, 2022). These swarms were relatively shallow and due to NW-SE extensional stresses. There is evidence for crustal fluids (Cherevatova *et al.*, 2015; Shiddiqi *et al.*, 2022), and these are considered to play a role in the development of the swarms (Shiddiqi *et al.*, 2022). Although the characteristics of the Sørfjorden swarm are common for the Nordland region, important insight may be obtained by examining whether changes in pore pressure and stress associated with tunnel leakage could act as a trigger mechanism.

Ground subsidence associated with large groundwater inflows during construction has been observed in several tunnels

excavated in basement rocks (Loew *et al.*, 2015; Wnuk *et al.*, 2019). Wnuk *et al.* (2019) observed deformation patterns using InSAR data similar to Sørfjorden, where the displacement field followed the tunnel trace. These deformations were explained by a reduction in pore pressure, which led to the closure of fractures around the tunnel. Loew *et al.* (2015) proposed that long-term rock mass deformation reduces the normal stress on faults as the rockmass between fractures compacts. Meanwhile, highly conductive fracture zones act as drainage pathways, connecting large volumes of rock to the tunnel.

It is commonly accepted that an increase in fluid pressure due to artificial injection (Ellsworth, 2013) or natural injection (Shelly *et al.*, 2016) can cause seismicity. Sibson (1981), based on geological field observations, presented the fault valve and pump models to explain how injection from an overpressured region can result in faulting accompanied by fluid movement. In the valve model, fluid overpressure at the base of the fault system drives the rupture, whereas in the pump model, rupture facilitates upward or lateral fluid migration from a high-pressure fault system to the lower pressured bedrock. The two mechanisms may also operate simultaneously (Marguin and Simpson, 2024). Either valving or pumping relies on a change in pressure gradient across a barrier. For example, Ross *et al.* (2020) postulate an increase in pressure in a fluid reservoir at depth. For the Hongtu tunnel in China, induced seismicity was linked to fluid migration caused by water inflow during tunnel construction (Ma *et al.*, 2025).

Given that earthquake swarms are typically triggered by fluids, the pressure and stress changes due to leakage are a prime candidate. To argue whether the Sørfjorden swarm was triggered in such a way, we consider whether the distance from the tunnel leakage and the time delay are realistic. Tunnel leakage occurred during the construction phase at a number of locations, in particular at crossings with significant weakness zones in the bedrock (Haugerud, 2020). There clearly is hydraulic conductivity through joints and fractures in the upper hundreds of meters (Haugerud, 2020). Although it is not clear how this conductivity extends to greater depths, faults and shear zones likely act as groundwater conduits. In this case, and provided we know the hydraulic diffusivity D of the fault zones, we can estimate, to first order, the diffusion time for perturbations in pore pressure p using

$$D\frac{\partial^2 p}{\partial x^2} = \frac{\partial p}{\partial t}, \tag{1}$$

resulting in a characteristic diffusion time of

$$t \approx \frac{x^2}{D}. \tag{2}$$

Estimates of D can be found in Guo *et al.* (2021), who obtained the hydraulic diffusivity of $D = [0.08 - 0.33]$ m^2/s for fault damage zones using a fault-guided flow model with tidal response of deep geothermal boreholes. If we insert this diffusivity range into the characteristic diffusion time equation with $x = 3000$ m, we get $t = [0.8–3.6]$ yr. This suggests that it would take between 1 and 4 yr for the pore-pressure perturbation to reach the swarm area, which is consistent with the observed delay of 3 yr.

Considering a pore-pressure diffusion model, both stress changes and pore-pressure variations act to modify the Coulomb stresses. Within the framework of poroelastic stress transfer in a 1D homogeneous medium (Segall and Lu, 2015), we can show that leakage increases tensional stresses near the swarm, consistent with our focal mechanisms and promoting Coulomb failure. In this model, pressure reduction inhibits failure, and thus pore-pressure diffusion may not explain the triggering of the swarm. However, the presence of conductive faults likely strongly modifies the pore-pressure distribution and stresses (Segall and Lu, 2015), making modeling in a homogeneous medium invalid in this context. Another possibility is that the increase in pressure differential drives the rupture, invoking models such as fault valving or pumping. In this scenario, we propose that after the initial barrier is broken, a combination of stress and fluid-pressure changes may have cascaded into the earthquake swarm. Ultimately, further modeling is required to test the relationship between leakage and seismicity suggested by the chronology of the different observations, but this is outside the scope of this study.

Conclusion

Based on the InSAR and seismological observations in conjunction with construction reports, we propose that the Sørfjorden swarm was triggered by a reduction in fluid pressure due to tunnel construction. InSAR-derived deformation patterns show localized subsidence along the tunnel between 2015 and 2019, consistent with leakage-induced pressure reduction in the surrounding rockmass. The temporal delay between the swarm and the tunnel construction is compatible with the time for a perturbation of pore pressure to diffuse within fault damage zones. We argue that the hypothesis of triggering by fluid leakage increasing the pressure differential at the swarm edges is sound, given the high water conductivity in the area, the knowledge that earthquake swarms are typically

triggered by fluid pressure changes, and the consistency of the valving/pumping model with cascading earthquakes. However, rigorous testing will require the development of heterogeneous poroelastic stress transfer models under different configurations given the high number of unknown parameters.

Data and Resources

Seismic waveform data are available via the UIB-NORSAR EIDA node web interface. We utilized data from the University of Bergen Seismic Network. The Sørfjorden swarm catalog is accessible through the ISC repository: doi: 10.31905/JA89PW86. Automatic detections were performed using the packages RobustRAQN and EQcorrscan (Chamberlain *et al.*, 2017). Figures were produced with PyGMT, Matplotlib, and Crameri scientific colormaps.

Declaration of Competing Interests

The authors acknowledge that there are no conflicts of interest recorded.

Acknowledgments

The NNSN operation and this work were supported by a Joint Industry Project through Offshore Norge. The authors thank Felix Halpaap and Kundan Kumar for their input. Constructive feedback from two reviewers and the associate editor helped improve and clarify our interpretation.

References

Chamberlain, C. J., C. J. Hopp, C. M. Boese, E. Warren-Smith, D. Chambers, S. X. Chu, K. Michailos, and J. Townend (2017). EQcorrscan: Repeating and near-repeating earthquake detection and analysis in Python, *Seismol. Res. Lett.* **89,** no. 1, 173–181.

Cherevatova, M., M. Y. Smirnov, A. Jones, L. B. Pedersen, M. Becken, M. Biolik, J. Ebbing, S. Gradmann, M. Gurk, J. Hübert, *et al.* (2015). Magnetotelluric array data analysis from north-west Fennoscandia, *Tectonophysics* **653,** 1–19.

Corfu, F., T. Andersen, and D. Gasser (2015). *The Scandinavian Caledonides: Main Features, Conceptual Advances and Critical Questions*, Geological Society, London, Special Publications Vol. 390, 9–43.

Dehls, J., Y. Larsen, P. Marinkovic, T. R. Lauknes, D. Stodle, and D. Moldestad (2019). INSAR. No: A National Insar deformation mapping/monitoring service in Norway—from concept to operations, *IGARSS 2019-2019 IEEE International Geoscience and Remote Sensing Symposium*, IEEE, 5461–5464.

Ellsworth, W. L. (2013). Injection-induced earthquakes, *Science* **341,** no. 6142, 1225942.

Farge, G., C. Jaupart, and N. M. Shapiro (2021). Episodicity and migration of low frequency earthquakes modeled with fast fluid pressure transients in the permeable subduction interface, *J. Geophys. Res. Solid Earth* **126,** no. 9, e2021JB021894, doi: 10.1029/2021JB021894.

Ferretti, A., C. Prati, and F. Rocca (2001). Permanent scatterers in SAR interferometry, *IEEE Trans. Geosci. Remote Sens.* **39,** no. 1, 8–20.

González, P. J., K. F. Tiampo, M. Palano, F. Cannavó, and J. Fernández (2012). The 2011 lorca earthquake slip distribution controlled by groundwater crustal unloading, *Nature Geosci.* **5,** no. 11, 821–825.

Gradmann, S., O. Olesen, M. Keiding, and Y. Maystrenko (2024). *The 3D Stress Field of Nordland, Northern Norway – Insights From Numerical Modelling*, Geological Society, London, Special Publications Vol. 546, 215–238.

Guo, H., E. E. Brodsky, T. H. W. Goebel, and T. T. Cladouhos (2021). Measuring fault zone and host rock hydraulic properties using tidal responses, *Geophys. Res. Lett.* **48,** no. 13, e2021GL093986.

Halpaap, F., L. Ottemöller, H. A. Shiddiqi, and S. Rondenay (2024). Lifecycle of an isolated seismic swarm in continental Southern Norway from nucleation, acceleration, and yielding to the demise of fault slip, *Seismol. Res. Lett.* **96,** no. 3, 1631–1644.

Hardebeck, J. L., and P. M. Shearer (2002). A new method for determining first-motion focal mechanisms, *Bull. Seismol. Soc. Am.* **92,** no. 6, 2264–2276.

Haugerud, H. J. (2020). Analysis on the extent of water inflow in the tunnel system of SmiSto Hydropower Project in Nordland, *Master's Thesis*, Norwegian University of Science and Technology, Department of Geoscience and Petroleum.

Hicks, E. C., H. Bungum, and C. D. Lindholm (2000). Seismic activity, inferred crustal stresses and seismotectonics in the Rana region, Northern Norway, *Quat. Sci. Rev.* **19,** no. 14, 1423–1436.

Lienert, B. R., E. Berg, and L. N. Frazer (1986). HYPOCENTER: An earthquake location method using centered, scaled, and adaptively damped least squares, *Bull. Seismol. Soc. Am.* **76,** no. 3, 771–783.

Loew, S., V. Lützenkirchen, J. Hansmann, A. Ryf, and P. Guntli (2015). Transient surface deformations caused by the Gotthard Base Tunnel, *Int. J. Rock Mech. Min. Sci.* **75,** 82–101.

Ma, X., C. Jiang, F. Yin, Z. Lv, Y. Qian, H. Zhai, T. Zhong, X. Yang, C. Jiang, and X. Yin (2025). Induced seismic swarm triggered by tunnel excavation and pore pressure diffusion mechanism, *Geophys. J. Int.* **243,** no. 2, ggaf364, doi: 10.1093/gji/ggaf364.

Marguin, V., and G. Simpson (2024). Numerical modelling of earthquake sequences involving valving and pumping of fluids, *Geophys. J. Int.* **238,** no. 1, 334–345.

McGarr, A., D. Simpson, and L. Seeber (2002). Case histories of induced and triggered seismicity, *Int. Geophys.* **81,** 647–661.

Prats-Iraola, P., R. Scheiber, L. Marotti, S. Wollstadt, and A. Reigber (2012). TOPS interferometry with terraSAR-X, *IEEE Trans. Geosci. Remote Sens.* **50,** 3179–3188.

Ross, Z. E., E. S. Cochran, D. T. Trugman, and J. D. Smith (2020). 3D fault architecture controls the dynamism of earthquake swarms, *Science* **368,** no. 6497, 1357–1361.

Segall, P., and S. Lu (2015). Injection-induced seismicity: Poroelastic and earthquake nucleation effects, *J. Geophys. Res. Solid Earth* **120,** no. 7, 5082–5103.

Shapiro, N. M., M. Campillo, E. Kaminski, J.-P. Vilotte, and C. Jaupart (2018). Low-frequency earthquakes and pore pressure transients in subduction zones, *Geophys. Res. Lett.* **45,** no. 20, 11–083.

Shelly, D. R., W. L. Ellsworth, and D. P. Hill (2016). Fluid-faulting evolution in high definition: Connecting fault structure and frequency-magnitude variations during the 2014 long valley caldera, california, earthquake swarm, *J. Geophys. Res. Solid Earth* **121,** no. 3, 1776–1795.

Shiddiqi, H. A., L. Ottemöller, S. Rondenay, S. Custódio, V. K. Gahalaut, R. K. Yadav, F. Halpaap, and K. Gahalaut (2023). Seismicity modulation due to hydrological loading in a stable continental region: A case study from the Jektvik swarm sequence in Northern Norway, *Geophys. J. Int.* **235,** no. 1, 231–246.

Shiddiqi, H. A., L. Ottemöller, S. Rondenay, F. Halpaap, S. Gradmann, and J. Michálek (2022). Crustal structure and intraplate seismicity in Nordland, Northern Norway: Insight from seismic tomography, *Geophys. J. Int.* **230,** 813–830.

Sibson, R. H. (1981). Fluid flow accompanying faulting: Field evidence and models, in *Earthquake Prediction: An International Review*, Vol. 4, 593–603.

Talwani, P. (1997). On the nature of reservoir-induced seismicity, *Pure Appl. Geophys.* **150,** 473–492.

Waldhauser, F. (2001). hypoDD: A program to compute double-difference hypocenter locations, *U.S. Geol. Surv. Open-File Rept. 01-113*.

Wetzler, N., E. Shalev, T. Göbel, F. Amelung, I. Kurzon, V. Lyakhovsky, and E. E. Brodsky (2019). Earthquake swarms triggered by groundwater extraction near the Dead Sea fault, *Geophys. Res. Lett.* **46,** no. 14, 8056–8063.

Wnuk, K., G. Walton, and W. Zhou (2019). Four-dimensional filtering of Insar persistent scatterers elucidates subsidence induced by tunnel excavation in the Sri Lankan highlands, *J. Appl. Remote Sens.* **13,** no. 3, 034508.

Woessner, J., and S. Wiemer (2005). Assessing the quality of earthquake catalogues: Estimating the magnitude of completeness and its uncertainty, *Bull. Seismol. Soc. Am.* **95,** no. 2, 684–698.

Wright, T. J., B. E. Parsons, and Z. Lu (2004). Toward mapping surface deformation in three dimensions using Insar, *Geophys. Res. Lett.* **31,** no. 1, doi: 10.1029/2003GL018827.

Manuscript received 24 October 2025
Published online 18 February 2026